Salvino Ciccariello

Dipartimento di Fisica "G.Galilei" e unita INFM,
Via F. Marzolo 8, 1-35131 Padova, Italy
ciccariello@pd.infn.it

The Small-angle Scattering Behaviour of a Regular Tetrahedron

Abstract
The correlation function of a regular tetrahedron, with edge lengths equal to L, is algebraically evaluated within the distance range [0, $\sqrt{3}L/2$]. In the remaining range [$\sqrt{3}L/2$, L] it must be evaluated numerically, and turns out to be negligible. The scattering intensity is numerically evaluated and compared to the sum of its first leading asymptotic terms, algebraically known as q^{-4}, q^{-6} and $q^{-6.5}$. The results indicate that polydisperse analyses in terms of tetrahedral particles could easily be made.

Key words: *tetrahedron, tetrahedral particles, polydisperse analysis, SAXS.*

Introduction

The scattering intensity from a statistically isotropic, monodisperse and dilute collection of equally shaped and homogeneous particles is proportional to the angular average of the square modulus of the Fourier transform (FT) of the function $\rho_p(r)$ that defines the particle's shape (and size). In fact, $\rho_p(r)$ is defined as being equal to unity if the top of r lies inside the particle, and equal to zero elsewhere. The full expression of the scattering intensity is found in Guinier & Fournet (1955) and Feigin & Svergun (1987)] presents euation (1), where N and $(n_1 - n_2)^2$ denote the total number of the particles present inside the sample and the sample's contrast respectively, $q = (4\pi/\lambda)\sin(\theta/2)$ is the modulus of the scattering vector q, and $\tilde{\omega}$ is a unit vector that ranges over all possible directions. The quantity inside the curly brackets is known as the isotropic form factor of the particle, and it will be denoted as $I_p(q)$ in the following. $I_p(q)$ can also be written as euation (2), where V_p is the particle volume and $\gamma_p(r)$ is the correlation function (CF) of the particle, defined as dependency (3).

This latter expression makes it evident that $\gamma_p(r)$ only depends on the geometrical shape as well as on the size D of the particle. In fact, the dependence on D is understood in the definition of $\rho_p(r)$. Consider now a collection of particles that have the same shape but different sizes, denoted by $D_1, \ldots, D_M$. Then, the function defining the geometry of the particle size D_j will be denoted by $\rho_p(r, D_j)$, which corresponds to

$$\rho_p(r, D_j) = \rho_p(r/D_j, 1), \qquad (4)$$

i.e. a scaling of r by $1/D_j$ converts the function defining the shape of the particle with unit size into the function defining the shape of the particle with size D_j. After substituting (4) for (3), one finds that $\gamma_p(r, D_j) = \gamma_p(r/D_j, 1)$ and, from Equation (2), that $I_p(q, D_j) = D_j^6 I_p(qD_j, 1)$. Under the same assumption used to get Equation (1), namely that interference effects between different particles are negligible, and the scattering intensity of a polydisperse and isotropic collection of particles with a given shape is

$$I(q) = (n_1 - n_2)^2 \sum_{j=1}^{M} N_j D_j^6 I_p(qD_j, 1). \qquad (5)$$

This result shows that it is possible to determine the particle size distribution (i.e. the set of pair values (D_j, N_j) for j=1,…,M) by best fitting the observed scattering intensity to Equation 5. To this end, it is important that the isotropic form factor of the particle with unit size be accurately known over a wide and very dense grid of q-values. This condition is certainly fulfilled if $I_p(qD_j, 1)$ is algebraically known. Unfortunately this happens only in the case of the spherical shape (Guinier & Fournet, 1955). This fact explains why so many analyses in terms of polydisperse spherical particles can be found in the scientific literature, even though in some cases, approximating the particles' shape to a sphere is rather dubious. These considerations show that efforts aimed at evaluating the form factors for other particle shapes in a closed algebraic form might be practically very useful. According to Equation (2), this goal can be achieved if one is able to evaluate the corresponding CFs algebraically. From these expressions, in fact, it should not be very hard to obtain accurate algebraic approximations which in turn allow us to evaluate their FTs in a closed algebraic form. At this point, it is important to note that particle shapes can be separated into two classes depending on whether a considered shape involves one or more than one size, respectively. Clearly, the first class contains the sphere and the five Platonic solids, i.e.: the tetrahedron, the cube, the octahedron, the dodecahedron and icosahedron. The second contains the other shapes, such as the cylinder, the ellipsoid and so on. For this reason, it is advisable first to perform a polydisperse analysis in terms of the Platonic shape which is more appropriate for the sample under analysis. Since the dodecahedral and the icosahedral shapes are already very similar to that of the sphere, and the octahedral shape is somewhat similar to the cubic one, it is important to have an accurate algebraic approximation of the CFs relevant to the cubic and the tetrahedral shape. We recall that

Equation 1, 2, 3 and 6.

$$I(q) = N(n_1 - n_2)^2 \left\{ \frac{1}{4\pi} \int d\tilde{\omega} \left| \int e^{iqr\cdot\tilde{\omega}} \rho_p(r) dv \right|^2 \right\} \qquad (1)$$

$$I_p(q) = \frac{4\pi V_p}{q} \int_0^\infty r \sin(qr) \gamma_p(r) dr \qquad (2)$$

$$\gamma_p(r) \equiv \frac{1}{4\pi V_p} \int d\tilde{\omega} \int \rho_p(r_1) \rho_p(r_1 + r\tilde{\omega}) dv_1 \qquad (3)$$

$$C_p(r) = -\frac{1}{\pi S} \int d\tilde{\omega} \int_S dS_1 \int_S dS_2 (\hat{\sigma}_1 \cdot \tilde{\omega})(\hat{\sigma}_2 \cdot \tilde{\omega}) \delta(r_1 + r\tilde{\omega} - r_2) \qquad (6)$$

some time ago Goodisman (1980) obtained the CF of a cubic particle in a closed form, while only very recently, Ciccariello (2005) obtained a closed-form expression of the intersect distribution of the tetrahedral particle. In this paper, as part of a more general work aimed at performing a polydisperse analysis with particles of cubic or tetrahedral shape, we shall restrict our attention to the last shape. Hence, in the chapter 'The SF of regular tetrahedron' we report the expression of the CF as well as its expansions around the points where the CF's derivatives behave discontinuously. The values of these discontinuities determine the asymptotic expansion of the isotropic form factor at large q-values, as will be detailed in the chapter 'The isotropic form factor of a regular tetrahedron'. The last section draws our final conclusions.

The CF of regular tetrahedron

As already mentioned, Ciccariello (2005) showed that $C_T(r)$, the intersect function of a regular tetrahedron, can be obtained in a closed algebraic form. According to Porod (1967), the intersect function $C_T(r)$ of a homogeneous particle is simply related to $\gamma''_p(r)$, the second derivative of the particle CF, as $C_p(r)=4V\gamma''(r)/S$, where V and S denote the volume and surface area of the particle. For a convex particle [i.e. a particle with a boundary such that any segment shares all of its points with the particle if its two ends lie on the boundary], $C_p(r)$ has a well-defined probabilistic meaning (Ciccariello, 2003), and the integral expression of $C_p(r)$ is (Ciccariello et al., 1981) given by (6).

Here the first integral is performed over all the possible directions of ϖ and the remaining two integrals over the particle surface. Moreover, the Dirac function $\delta(?)$ requires that the two infinitesimal surface elements dS_1 and dS_2, located at r_1 and r_2, be separated by the vector $r\varpi$. Finally, σ_1 and σ_2 are two unit vectors perpendicular to dS_1 and dS_2 and pointing outwardly to the particle. Specifying Equation 6 to a regular tetrahedron with an edge length equal to unity, the integral can be explicitly evaluated. One finds that the algebraic expression of $C_T(r)$ depends on value r. In fact, the allowed range of distances [0,1] splits into the five intervals: $[0, 1/\sqrt{2}]$, $[1/\sqrt{2},\sqrt{2/3}]$, $[\sqrt{2/3},\sqrt{3}/2]$, $[\sqrt{3}/2, \sqrt{7}/3]$ and $[\sqrt{7}/3, 1]$ labelled by I,..,V. The corresponding $\gamma_T''(r)$ expressions will be denoted as $\gamma_I''(r)$, …, $\gamma_V''(r)$ omitting subscript T. Within the three inner intervals, the functional dependence on r of $\gamma_a''(r)$, with a= 1,2,3 is

$$\gamma_a''(r) = A_a + S_a r + B_a / r^3 , \qquad (7a)$$

with a = I, II, III,

where the involved numerical coefficients are different and dependent on the relevant r-interval as specified below

$$\begin{cases} A_I \equiv 12\sqrt{2}\left[1+\left(\pi - arccos(1/3)\right)/2\sqrt{2}\right]/\pi , \\ S_I \equiv -3\left(6+5\sqrt{3}\pi\right)/2\sqrt{2}\pi \\ B_I \equiv 0, \end{cases} \qquad (7a.1)$$

$$\begin{cases} A_{II} \equiv A_I - 12, \\ S_{II} \equiv S_I + 9\sqrt{2}, \\ B_{II} \equiv 3/2\sqrt{2}, \end{cases} \qquad (7a.2)$$

and

$$\begin{cases} A_{III} \equiv A_{II} - 12, \\ S_{III} \equiv S_{II} + 9\sqrt{3/2}, \\ B_{III} \equiv B_{II} + 2\sqrt{2/3}. \end{cases} \qquad (7a.3)$$

Equation 7b, 7c, 9a, 9b and 9c.

$$\gamma''_{IV}(r) = \frac{1}{12\pi r^3}\left\{\pi\left(9\sqrt{2}-16\sqrt{6}\right) - r^2\left[18\sqrt{2}\left(3\pi+5\Delta_3\right)\right] + 72r^3\left[\sqrt{8}-4\pi-\arccos\left(1/3\right)\right] + \sqrt{8}r^4\left[-27+108\pi+67\sqrt{3}\pi\right] + \right. \qquad (7.b)$$
$$+\sqrt{2}\left[32\sqrt{3}\arccos\left[\frac{\sqrt{27}\left(1-r^2\right)\Delta_3}{2{\Delta_2}^3}\right] - 9\arccos\left[\frac{7-12r^2+4r^4}{{\Delta_1}^4}\right] + 24\sqrt{3}\arccos\left[\frac{7-9\Delta_3 9r^2\left(\Delta_3-1\right)}{4{\Delta_2}^3}\right]\right] + 54\sqrt{2}r^2\left[4\arccos\left[\frac{1-\Delta_3}{2\Delta_1}\right] + \right.$$
$$\left. + \arccos\left[\frac{7-12r^2+4r^4}{{\Delta_1}^4}\right]\right] + 144r^3\left[\arccos\left[\frac{-\sqrt{2}\Delta_3}{\sqrt{3}\Delta_2{\Delta_1}^2}\right] + \arccos\left[\frac{2-r^2-2r^4}{2-7r^2+6r^4}\right]\right] + 6\sqrt{2}r^4\left[2\sqrt{3}\arccos\left[\frac{3-2r^2}{2r^2}\right] - 9\sqrt{3}\arccos\left[\frac{\Delta_3}{2r}\right] + \right.$$
$$\left. \left. - 72\arccos\left[\frac{1-\Delta_3}{2\Delta_1}\right] - 16\sqrt{3}\arccos\left[\frac{\sqrt{3}\left(\Delta_3+2r^2-3\right)}{4r^2}\right] - 9\sqrt{3}\arccos\left[\frac{7-9\Delta_3+9r^2\left(\Delta_3-1\right)}{4{\Delta_2}^3}\right]\right]\right\}$$

$$\gamma''_{V}(r) = \frac{1}{12\pi r^3}\left\{8\sqrt{6}\pi - 90\sqrt{2}r^2\Delta_3 + 72r^3\left(\sqrt{8}-\arccos\ \frac{1}{3}\right) - 18\sqrt{2}r^4\left(3-\pi\left(12-\sqrt{3}\right)\right) + \left[16\sqrt{6}\arccos\left[\frac{9r^2-7}{2{\Delta_2}^3}\right]\right.\right. - \qquad (7.c)$$
$$+ 9\sqrt{2}\arccos\left[\frac{-7+12r^2-4r^4}{{\Delta_1}^4}\right] - 24\sqrt{6}\arccos\left[\frac{3\Delta_3-1}{4\Delta_2}\right]\left.\right] - 144r^3\left[\arccos\left[\frac{-3-r^2+6r^4+\Delta_3\left(1-9r^2+6r^4\right)}{\sqrt{3}{\Delta_1}^3\Delta_2\sqrt{1+6r^2-\Delta_3}}\right] + \right.$$
$$\left. \left. - \arccos\left[\frac{\sqrt{2}\left[-2+15r^2+13r^4-36r^6+\Delta_3\left(2+9r^2-9r^4\right)\right]}{\Delta_1{\Delta_2}^2\sqrt{1+6r^2-\Delta_3}\left(1+6r^2+\Delta_3\right)}\right]\right] + 54r^4\left[\sqrt{6}\arccos\left[\frac{\Delta_3\left(9-36r^2+46r^4-18\ r^6\right)}{2r^5{\Delta_2}^3}\right] - 8\sqrt{2}\arccos\left[\frac{1-\Delta_3}{2\Delta_1}\right]\right]\right\}$$

$$\gamma''_{II}(r) = g_{2,0} - g_{2,1}(r_2-r) + g_{2,2,R}\left(r_2-r\right)^2 + g_{2,3,R}\left(r_2-r\right)^3 + O\left(\left(r_2-r\right)^4\right) \qquad (9.a)$$

$$\gamma''_{III}(r) = g_{2,0} - g_{2,1}(r-r_2) + g_{2,2,R}\left(r-r_2\right)^2 + g_{2,3,R}\left(r-r_2\right)^3 + O\left(\left(r-r_2\right)^4\right) \qquad (9.b)$$

$$g_{2,0} \equiv -3\left(19\sqrt{3}-44+8\left(\sqrt{32}-\sqrt{3}+2\arcsin 3\right)/\pi\right)/8, \quad g_{2,1} \equiv 3\left(24+\left(20\sqrt{3}-21\right)\pi\right)/8\sqrt{2}\pi , \qquad (9.c)$$

$$g_{2,2,L} \equiv 81\sqrt{3}/8, \quad g_{2,3,L} \equiv 405/8\sqrt{2}, \quad g_{2,2,R} \equiv 27+81\sqrt{3}/8, \quad g_{2,3,R} \equiv -45\left(9+8\sqrt{3}\right)/8\sqrt{2}. \qquad (9.d)$$

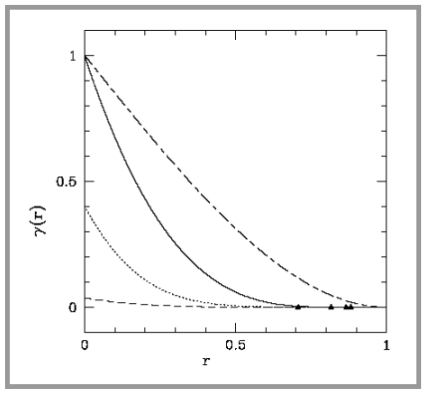

Figure 1. *The continuous and the dash-dotted curves plot the CFs of a regular tetrahedron with unit edge and of a sphere with unit diameter respectively. The sharper decrease of the first, compared to that of the second, should be noted. The black triangles have the following coordinates: $1/\sqrt{2}$, $\sqrt{2/3}$, $\sqrt{3}/2$, and $\sqrt{7}/3$. The dotted and the broken curves respectively plot the tetrahedron CF, multiplied by 100 and 1000, within the intervals $[1/\sqrt{2}, 1]$ and $[\sqrt{3}/2, 1]$ (both scaled to the interval [0, 1]).*

In the outer two r-intervals, one finds (Eq. 7.b) and respectively, (Eq. 7c) where

$$\Delta_1 \equiv \sqrt{2r^2-1}, \quad \Delta_2 \equiv \sqrt{3r^2-2}, \quad \Delta_3 \equiv \sqrt{4r^2-3}. \tag{7.d}$$

Expressions (7.a) - (7.c) can easily be expanded around the end points of the relevant r-intervals. Putting $r_1 \equiv 1/\sqrt{2}, .., r_5 \equiv 1$, one can find in the left neighbourhood of r_1 that

$$\gamma_I''(r) = g_{1,0} + g_{1,1}(r_1 - r) \tag{8.a}$$

and in the right neighbourhood that

$$\gamma_{II}''(r) = g_{1,0} - g_{1,1}(r - r_1) + g_{1,2,R}(r - r_1)^2 + g_{1,3,R}(r - r_1)^3 + O\left((r - r_1)^4\right) \tag{8.b}$$

with $g_{1,0} \equiv A_I + S_I/\sqrt{2}$, $g_{1,1} \equiv -S_I$, $g_{1,2,R} \equiv 36$ and $g_{1,3,R} \equiv -60\sqrt{2}$. These coefficients show that $\gamma''(r)$ and $\gamma^{(3)}(r)$ are continuous at $r=r_1$, while the subsequent derivatives $\gamma^{(4)}(r)$ and $\gamma^{(5)}(r)$ present finite discontinuities respectively equal to $2g_{1,2,R}$ and $6\,g_{1,3,R}$. Similarly, in the left and right neighbourhoods of r_2, one finds (Eq. 9a) and respectively, (Eq. 9b) with (Eq. 9c).

Hence, the discontinuity of $\gamma^{(4)}(r)$ at $r=r_2$ is $2(g_{2,2,R} - g_{2,2,L}) = 54$ and that $\gamma^{(5)}(r)$ is $6(g_{2,3,R} - g_{2,3,L}) = -270\sqrt{3/2}$.

Around r_3, the left and right expressions read

$$\gamma_{III}''(r) = g_{3,0} - g_{3,1}(r_3 - r) + g_{3,2}(r_3 - r)^2 + g_{3,3}(r_3 - r)^3 + O\left((r_3 - r)^4\right) \tag{10a}$$

and

$$\gamma_{IV}''(r) = g_{3,0} - g_{3,1}(r_3 - r) + g_{3,2}(r_3 - r)^2 + g_{2,5/2,R}(r - r_3)^{5/2} g_{\overline{3,3}}(r - r_3)^3 + O\left((r_3 - r)^{5/2}\right) \tag{10.b}$$

with

$$g_{3,0} = \left(-1296 + 209\sqrt{2} + 372\sqrt{6} - 54\left(3\sqrt{6} - 16\sqrt{2} + 8\,arc\cos(1/3)\right)/\pi\right)/72,$$

$$g_{3,1} = -\left(5\sqrt{2} - 101/6\sqrt{6} - 9/\sqrt{2}\pi\right),$$

$$g_{3,2} = 16\sqrt{2}\left(8 + \sqrt{27}\right)/9 \quad \text{and}$$

$$g_{2,5/2,R} = -1024\sqrt{2}/3^{1/4}5\pi.$$

Hence, at $r=r^3$, γ'', $\gamma^{(3)}$and $\gamma^{(4)}$ are continuous. But $\gamma^{(5)}(r)$ approaches a finite value as $r \to r_3^-$ from the left, and shows an algebraic singularity as $r \to r_3^+$ from the right, since

$$\gamma^{(5)}(r) \approx 15 g_{2,5/2,R} \Big/ \left(8(r - r_3)^{1/2}\right) \quad \text{as } r \to r_3^+. \tag{10.c}$$

Around r_4, the left and right expansions of $\gamma''(r)$ were evaluated up to the tenth term, and they turn out to be equal. This strongly indicates that $\gamma_{IV}''(r)$ and $\gamma_V''(r)$, despite their analytically different forms, are the same function.

Finally, around r_5, one finds that

$$\gamma_V''(r) = g_{5,3,L}(r_5 - r)^2 + O\left((r_5 - r)^4\right), \tag{11}$$

with $g_{5,3,L} \equiv 24\sqrt{2}/\pi$. Since $\gamma''(r) \equiv 0$ if $r > 1$, one concludes that γ'', $\gamma^{(3)}$ and $\gamma^{(4)}$ are continuous at $r=r_5$, while $\gamma^{(5)}(r)$ has a finite discontinuity equal to $6\gamma_{5,3,L}$ at r_5. These results will be used in the following section in order to obtain the leading terms of the asymptotic expansion of $I_T(q)$.

Now we will discuss how the CF of a regular tetrahedron can be obtained from equations 7a-7e. Recalling the normalisation condition $\gamma(0)=1$ and Porod's (1951) relation $\gamma'(0) = -S/4V$, the CF function is given by

$$\gamma(r) = 1 - (S/4V)r + \int_0^r dx \int_0^x \gamma''(y)dy = 1 - (S/4V)r + \int_0^r (r - y)\gamma''(y)dy. \tag{12}$$

Simple calculation yields

$$\gamma_T(r) = \gamma_I(r) \equiv 1 - (S/4V)r + A_I r^2/2 + S_I r^3/6 \quad \text{if } 0 < r < r_1, \tag{13.a}$$

$$\gamma_T(r) = \gamma_{II}(r) \equiv \gamma_I(r_1) + \gamma_I'(r_1)(r - r_1) + A_{II}(r - r_1)^2/2 + S_{II}(r - r_1)^2(r + \sqrt{2})/6 + \sqrt{2}B_{II}(r - r_1)^2/r \quad \text{if } r_1 < r < r_2 \tag{13.b}$$

$$\gamma_T(r) = \gamma_{III}(r) \equiv \gamma_{II}(r_2) + \gamma_{II}'(r_2)(r - r_2) + A_{III}(r - r_2)^2/2 + S_{III}(r - r_2)^2(r + 2r_2)/6 + 3B_{III}(r - r_2)^2/4r \quad \text{if } r_2 < r < r_3, \tag{13.c}$$

$$\gamma_T(r) = \gamma_{IV}(r) \equiv \gamma_{III}(r_3) + \gamma_{III}'(r_3)(r - r_3) + \int_{r_3}^r (r - y)\gamma_{IV}''(y)dy \quad \text{if } r_3 < r < r_4 \tag{13.d}$$

and

$$\gamma_T(r) = \gamma_V(r) \equiv \gamma_{IV}(r_4) + \gamma_{IV}'(r_4)(r - r_4) + \int_{r_4}^r (r - y)\gamma_V''(y)dy \quad \text{if } r_4 < r < r_5 \tag{13.e}$$

Therefore, the CF is algebraically known within the three inner ranges of distances and it must be numerically evaluated by (13d) and (13e) within the two outer ranges. Figures 1, 2a, 2b, 3a and 3b re-

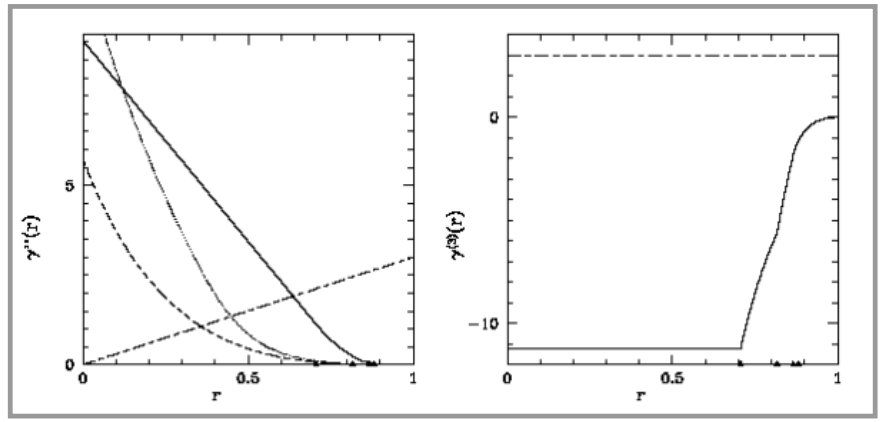

Figure 2. *(a) The continuous and the dash-dotted curves plot the second derivatives of the CFs of a unit regular tetrahedron and a unit sphere. The behaviours of the two are radically different. The first is different from zero at r = 0 because the tetrahedron is an angular body, while the second is equal to zero because the sphere has no edges. Moreover, the first monotonously decreases, while the second increases. The dotted and the broken curves respectively are the plots of $\gamma_T''(r)$, multiplied by 10 and 100, within the intervals $[1/\sqrt{2}, 1]$ and $[\sqrt{3}/2, 1]$ (scaled to the interval [0, 1]). The above scaling factors are smaller than those of Figure 1 by one order of magnitude. Plots of $\gamma_T^{(5)}(r)$, and $\gamma_3^{(5)}(r)$, The second is constant everywhere, while the first is continuous everywhere and constant only within the first range of distances.*

spectively show the plots of $\gamma_T(r)$, $\gamma_T''(r)$, $\gamma_T^{(3)}(r)$, $\gamma_T^{(4)}(r)$ and $\gamma_T^{(5)}(r)$. The dotted and the broken lines in Figure 1 are the plots of the CF, multiplied by 100 and 1000, within the r-intervals $[1/\sqrt{2}, 1]$ and $[\sqrt{3}/2, 1]$, scaled to the interval [0,1]. This shows that the CF of the tetrahedron is very small within the interval $[\sqrt{3}/2, 1]$ where its analytical expressions, given by equations 7b and 7c, are more involved. Figure 2a also shows that the intersect function of the tetrahedron is radically different from that of the sphere. Moreover, its shape is similar to that found by Smarsly et al. (2002) for some activated carbons (see, in particular, their Figure 6). This similarity indicates that the angularity [Porod 919670, Mering & Tchoubar (1968) and Ciccariello (1997)] of the interfaces is a crucial structural parameter for some samples. It is also recalled that the second derivative of the CF of a particle, whatever its shape, obeys the following sum-rules (Gille, 2000)

$$\int_0^1 \gamma_p''(r)dr = -\gamma_p'(0) = S/4V_p, \quad (14a)$$

$$\int_0^1 r\gamma_p''(r)\,dr = 1, \quad (14b)$$

$$\int_0^1 r^4\gamma_p''(r)\,dr = 3V_p/\pi\,. \quad (14c)$$

For the tetrahedron, we found that the values of the integrals on the left hand sides of (14a)-(14c), evaluated using a numerical grid with 10^5 points, coincide with the right hand side (rhs) values up to the fifth digit (included). This check make us confident that no numerical mistake occurred in working out Equations 7a-7d.

The isotropic form factor of a regular tetrahedron

We now introduce the dimensionless isotropic form factor, defined as $\tilde{I}_T(q) = I_T(q)/V_T$. From Equation 2 and Equations 13a-e, it follows that (Eq. 15).

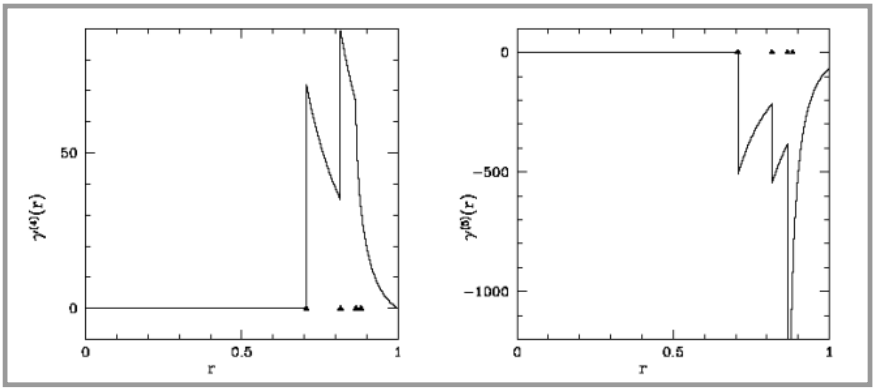

Figure 3. *(a) Plot of the fourth derivative of the tetrahedron CF. The finite discontinuities at $r=1/\sqrt{2}$ and $\sqrt{2/3}$ are evident. (b) The subsequent derivative $\gamma_T^{(5)}(r)$ shows finite discontinuities at the previous two points and at r=1, and is negatively divergent as $r \to (\sqrt{3}/2)^+$.*

With $r_0 \equiv 0$ and $\gamma_1(r) \equiv \gamma_I(r), \ldots, \gamma_5(r) \equiv \gamma_V(r)$. Owing to the algebraic expressions of the CF within the three inner intervals [see equations (13a)-(13d)], it is evident that the integrals corresponding to j=1,2,3 in Equation 15) can be algebraically calculated. On the contrary, the remaining two integrals (corresponding to j=4, 5) must be evaluated numerically since $\gamma_{IV}(r)$ and $\gamma_V(r)$ are only known numerically. However, the knowledge of $\gamma_{IV}(r)$ and $\gamma_V(r)$ allows us to work out a convenient approximation of $\gamma_T(r)$ within the interval $r_3<r<r_5$ and by Fourier-transforming this approximation, we can obtain an algebraic expression of the FT of the full $\gamma_T(r)$. On one hand, it should not be difficult to work out a polynomial approximation of $\gamma_T(r)$ within the interval $[r_3, r_5]$, because $\gamma_T(r)$ is here rather small. On the other hand, in working out this approximation, it is important that the values of the first discontinuities of the derivatives be preserved, otherwise the first leading terms of the asymptotic expansion of $I_T(q)$ will not be reproduced. In this paper we shall confine ourselves to deriving the expressions of these terms. After putting $\Gamma_j(r) \equiv r\gamma_j(r)$, the *j*th integral present in Equation 15) takes the form

$$F_j(q) = \int_{r_{j-1}}^{r_j} \sin(qr)\Gamma_j(r)dr.$$

Five subsequent integrations by parts yield the following: (Eq.16).

Since $\Gamma_j^n(r) = r\gamma_j^{(n)}(r) + r\gamma_j^{(n-1)}(r)$, from the above reported properties of the $\gamma_j^{(n)}(r)$s [see equations (8)-(11)] one concludes that $\Gamma_j^5(r)$= is continuous within the relevant integration domain $[r_{j-1}, r_j]$ if j=1,2,3,5. In the remaining case j=4 we know that (Eq. 17) as $r \to r_3^+$.

Equation 15, 16, 17, 18 and 19.

$$\tilde{I}_T(q) = \frac{4\pi}{q}\int_0^\infty r\sin(qr)\gamma_T(r)dr = \frac{4\pi}{q}\sum_{j=1}^{5}\int_{r_{j-1}}^{r_j} r\sin(qr)\gamma_j(r)dr \quad (15)$$

$$F_j(q) = -\frac{\cos(qr)}{q}\Gamma_j(r)\Big|_{r_{j-1}}^{r_j} + \frac{\sin(qr)}{q^2}\Gamma_j'(r)\Big|_{r_{j-1}}^{r_j} + \frac{\cos(qr)}{q^3}\Gamma_j''(r)\Big|_{r_{j-1}}^{r_j} - \frac{\sin(qr)}{q^4}\Gamma_j^{(3)}(r)\Big|_{r_{j-1}}^{r_j} - \frac{\cos(qr)}{q^5}\Gamma_j^{(4)}(r)\Big|_{r_{j-1}}^{r_j} + \frac{1}{q^5}\int_{r_{j-1}}^{r_j}\cos(qr)\Gamma_j^{(5)}(r)dr. \quad (16)$$

$$\Gamma_4^{(5)}(r) = r\gamma_4^{(5)}(r) + n\gamma_4^{(4)}(r) \approx \frac{\left(15g_{2,5/2,R}\right)r}{8(r-r)_3^{1/2}} \qquad \text{as } r \to r_3^+ \quad (17)$$

$$\tilde{I}_q(q) \approx -\frac{8\pi\gamma_T'(0)}{q^4} + \frac{16\pi\gamma_T^{(3)}(0)}{q^6} + \frac{4\pi}{q^6}\left[r_1\cos(qr_1)\left[\gamma_2^{(4)}\left(r_1^+\right) - \gamma_1^{(4)}\left(r_1^-\right)\right] + r_2\cos(qr_2)\left[\gamma_3^{(4)}(r_2^+) - \gamma_2^{(4)}(r_2^-)\right]\right] + o(q^{-6}) = \quad (18)$$

$$= \frac{2\pi S}{Vq^4} + \frac{16\pi S_I}{q^6} + \frac{4\pi}{q^6}\left[\frac{72\cos\left(q/\sqrt{2}\right)}{\sqrt{2}} + 54\sqrt{2/3}\cos\left(q\sqrt{2/3}\right)\right] + o(q^{-6}).$$

$$\tilde{I}_T(q) \approx \frac{2\pi S}{Vq^4} + \frac{16\pi S_I}{q^6} + \frac{4\pi}{q^6}\left[\frac{72\cos\left(q/\sqrt{2}\right)}{\sqrt{2}} + 54\sqrt{2/3}\cos\left(q\sqrt{2/3}\right)\right] - \frac{768\sqrt{2\pi}3^{1/4}}{q^{6.5}}\cos\left(q\sqrt{3}/2 + \pi/4\right) + O\left(q^{-7}\right) \quad (19)$$

This power law singularity does not prevent the existence of the integral

$$\int_{r_3}^{r_4} \cos(qr)\Gamma_4^{(5)}(r)\,dr,$$

but the determination of the asymptotic behaviour of this integral deserves some attention, as will become clear later. For the moment, it is sufficient to anticipate that this integral decreases asymptotically as $q^{-1/2}$. For the cases $j \neq 4$, the integral

$$\int_{r_j-1}^{r_j} \cos(qr)\,\Gamma_j^{(5)}(r)dr$$

defines a function of q that decreases as q^{-1} at large qs, because it can still be integrated by parts. Hence, on the rhs of (16), the term involving the integral decreases faster than the remaining ones. Consequently, from (15), one concludes that the sum of the last terms, divided by q, determines the asymptotic expansion of $\tilde{I}(q)$ up to the terms $O(1/q^6)$. In evaluating the sum, we should observe that each r_j, with $j \neq \{0,5\}$, appears as an upper limit for $F_j(q)$ and as a lower limit for $F_{j+1}(q)$. Hence, the corresponding contributions relevant to a derivative of order n cancel out, unless the derivative is discontinuous at r_j. Therefore, we must consider only the points where the derivatives are discontinuous and the end points r_0 and r_5. In this way, we find that (Eq. 18).

For completeness we now derive the asymptotic behaviour of

$$\int_{r_3}^{r_4} \cos(qr)\,\Gamma_4^{(5)}(r)\,dr.$$

The integrand has a power-law singularity, reported in Equation 17, at $r = r_3$ and it is analytic in the remaining points of the integration domain. Then, one uses Equations 4 and 5 reported on page 48 of Erdély (1956) to obtain the following asymptotic relation:

$$\int_{r_3}^{r_4} \cos(qr)\Gamma_4^{(5)}(r)dr \approx$$
$$-\Re\left(\Gamma(1/2)Ce^{i\pi(1/2-2)/2}e^{iqr_3}q^{-1/2}\right)$$

where R denotes the real part, $\Gamma(\cdot)$ the Euler gamma function and $C \equiv 15r_3 g_{2,5/2,R}/8$. In this way the asymptotic expansion of $\tilde{I}(q)$ up to the term $O(q^{-6-1/2}\})$ is (Eq. 19).

Figure 4 shows the form factor (continuous curve) of the tetrahedrons and, for comparison, that of a sphere with diameter equal to the tetrahedron edge. As expected on the basis of Guinier's law, the first decreases more slowly than the second, and one would naively conclude that no further differences occur. However, the differences are hidden in the tail's behaviour. This is already evident from the Porod plot of the tetrahedron intensity shown in Figure 5. In contrast to the case of the sphere, one observes mild oscillations that fade at large q's. Moreover, the curve mostly lies below the Porod plateau. This is a consequence of the large angularity of the tetrahedron (Ciccariello et al., 1981). Once one has subtracted the Porod and the (generalised) Kirste-Porod [Kirste & Porod (1962), Ciccariello & Sobry (1995)] term from $\tilde{I}(q)$, i.e. the first and second term reported on the rhs of (19), the resulting quantity oscillates around zero and decreases as q^{-6}. This is made evident in Figure 6a by the dotted curve that is the Kirste-Porod plot of the aforesaid quantity. After subtracting the $O(q^{-6})$ oscillatory contributions from this, the resulting quantity, multiplied by q^6, will decrease as $q^{-0.5}$, as shown in Figure 6a by the continuous curve coinciding with the dotted curve in Figure 6b. Once we further subtract the term decreasing as $q^{-6.5}$, the remaining quantity will decrease as q^{-7} and the oscillations in the corresponding Kirste-Porod plot will fade as q increases. The continuous curve of Figure 6b makes this behaviour evident.

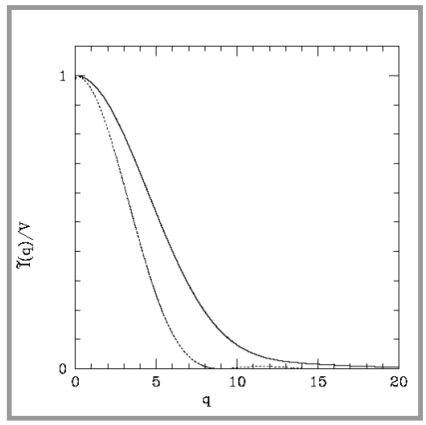

Figure 4. *The continuous and the dotted curves are the plots of the isotropic form factors (normalised to 1 at q=0) of a unit regular tetrahedron and a unit sphere. The sharper decrease of the second intensity near the origin reflects the fact that the Guinier gyration radius of the sphere is larger than that of the tetrahedron. Moreover, the sphere intensity presents, at q ≈ 12, a small peak which is absent in the tetrahedron intensity.*

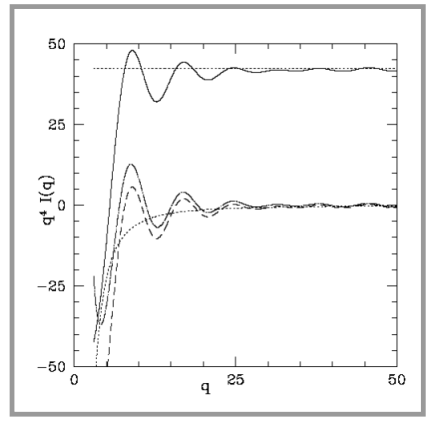

Figure 5. *The continuous curve is the Porod plot of $I_T(q)$, and the horizontal dotted line shows the Porod plateau [for clarity reasons, the two curves have been vertically shifted by -50]. The lower dotted curve is the Kirste-Porod contribution, the broken curve is the Porod plot of the intensity subtracted of the Porod $O(q^{-4})$ contribution, and the long dash curve is the Porod plot of the intensity subtracted of the Porod and the (generalised) Kirste-Porod $O(q^{-6})$ terms. This curve clearly oscillates around the zero value.*

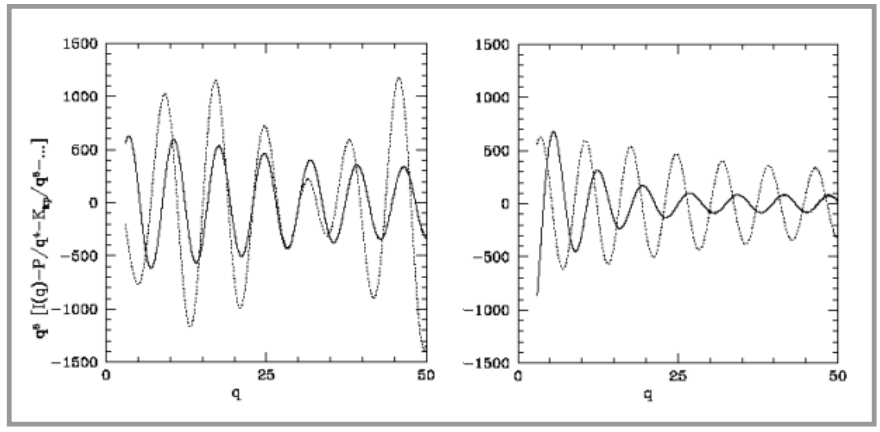

Figure 6. *The two figures show the Kirste-Porod (KP) plots of $\tilde{I}_T(q)$ the tetrahedron intensity, subtracted from some contributions. In particular, on the left, the broken curve is the KP plot of $\tilde{I}_T(q)$ minus the Porod O(q-4) and the Kirste-Porod O(q-6) terms (i.e. the first two terms on the rhs of (19), while the continuous curve is the KP plot obtained by subtracting the two O(q-6) terms from the former quantity also. On the right, the dotted curve is the continuous curve of the left figure, while the continuous one is the KP plot of the residual term denoted by O(q-7) in Equation 19.*

Conclusions

The results reported in the previous two sections show that a polydisperse analysis of the intensity relevant to an isotropic sample made up of homogeneous tetrahedral particles is feasible. In fact, the results of §3 show that the leading asymptotic terms, up to the $O(q^6)$ contributions included, accurately describe the scattering intensity in the tail region. The previous terms are only related to the tetrahedron CF evaluated within the interval $[0, \sqrt{3}]$. Here the CF is algebraically known, and the same happens for its Fourier transform. On the other hand, the broken curve of Figure 1 shows that the CF is negligible within the complementary interval $[\sqrt{3}, 1]$m and can be neglected without affecting the asymptotic behaviour of $\tilde{I}_T(q)$ if one neglects the terms decreasing faster than $q^{-6.5}$. One concludes that the FT of $\gamma_T(r)$, restricted to $[0,\sqrt{3}]$, is quite accurate and algebraically known. Hence, polydisperse analyses in terms of tetrahedral particles should be easily feasible.

References

1. *Ciccariello, S. (1997). X-ray investigations of polymer structures Edited by A. Włochowicz, Proc. SPIE-The International Society for Optical Engineering* ***3095****, 142-156.*
2. *Ciccariello, S. (2003). Acta Cryst.* ***A59****, 506-512.*
3. *Ciccariello, S. (2005). J. Appl. Cryst.* ***38****, 97-106.*
4. *Ciccariello, S. & Sobry, R. (1995). Acta Cryst. A****51****, 60-69.*
5. *Ciccariello, S., Cocco, G., Benedetti, A. & Enzo, S. (1981). Phys. Rev. B****23****, 6474-6485.*
6. *Erdéley, A. (1956). Asymptotic expansions. New York: Dover.*
7. *Feigin, L.A. & Svergun, D.I. (1987). Structure Analysis by Small-Angle X-ray and Neutron Scattering. New York: Plenum Press.*
8. *Gille, W. (2000). Eur. Phys. Journ. B****17****, 371-383*
9. *Goodisman, J. (1980). J. Appl. Cryst.* ***13,*** *132-134*
10. *Guinier, A. & Fournet, G. (1955). Small-angle scattering of x-rays, New York: Wiley.*
11. *Kirste, R & Porod, G. (1962). Kolloid Zeit.* ***184****, 1-6.*
12. *Mering, J. & Tchoubar, D. (1968). J. Appl. Cryst.* ***1****, 153-165.*
13. *Porod, G. (1951). Kolloid Z.* ***124****}, 83-114.*
14. *Porod, G. (1967). Small-angle X-ray scattering. Proceedings of the Syracuse Conference}, Edited by H. Brumberger, pp. 1-15. New York: Gordon and Breach.*
15. *Smarsly, B., Antonietti, M. & Wolff, T. (2002). J. Chem. Phys.* ***116****, 2618-2627.*

Received 08.12.2004 Reviewed 10.02.2005